Reciprocal space tomography of 3D skyrmion lattice order in a chiral magnet

Shilei Zhang[a], Gerrit van der Laan[b], Jan Müller[c], Lukas Heinen[c], Markus Garst[d], Andreas Bauer[e], Helmuth Berger[f], Christian Pfleiderer[e], and Thorsten Hesjedal[1,a]

[a]Clarendon Laboratory, Department of Physics, University of Oxford, Oxford, OX1 3PU, UK; [b]Magnetic Spectroscopy Group, Diamond Light Source, Didcot, OX11 0DE, UK; [c]Institut für Theoretische Physik, Universität zu Köln, 50937 Köln, Germany; [d]Institut für Theoretische Physik, TU Dresden, 01062 Dresden, Germany; [e]Physik-Department, Technische Universität München, 85748 Garching, Germany; [f]Ecole Polytechnique Fédérale de Lausanne (EPFL), CH-1015 Lausanne, Switzerland

This manuscript was compiled on April 23, 2018

It is commonly assumed that surfaces modify the properties of stable materials within the top few atomic layers of a bulk specimen only. Exploiting the polarization dependence of resonant elastic x-ray scattering to go beyond conventional diffraction and imaging techniques, we have determined the depth dependence of the full three-dimensional spin structure of skyrmions, i.e., topologically non-trivial whirls of the magnetization, below the surface of a bulk sample of Cu_2OSeO_3. We found that the skyrmions change exponentially from pure Néel- to pure Bloch-twisting over a distance of several hundred nanometers between the surface and the bulk, respectively. Though qualitatively consistent with theory, the strength of the Néel-twisting at the surface and the length scale of the variation observed experimentally exceed material-specific modeling substantially. In view of the exceptionally complete quantitative theoretical account of the magnetic rigidities and associated static and dynamic properties of skyrmions in Cu_2OSeO_3 and related materials, we conclude that subtle changes of the bulk properties must exist at distances up to several hundred atomic layers into the bulk, which originate in the presence of the surface. This has far-reaching implications for the creation of skyrmions in surface-dominated systems, and identifies, more generally, surface-induced gradual variations deep within a bulk material and their impact on tailored functionalities as an unchartered scientific territory.

skyrmions | resonant elastic x-ray scattering | 3D magnetic imaging | magnetic surface effects | spintronics | Cu_2OSeO_3

An extraordinary variety of experimental and theoretical tools has made the exploration and technological exploitation of surfaces of bulk materials one of the most thriving topics in the natural sciences (1, 2). As the underlying interactions and associated effects of charge screening occur on atomic distances, it is broadly assumed that surfaces do not modify the bulk properties of inherently stable materials beyond the top few atomic layers. Moreover, only a few studies have addressed the evolution of materials properties with atomic resolution far below surfaces, since conventional methods do not provide the necessary information (3–5).

The local orientation and magnitude of the magnetization in spin textures is particularly amenable to track gradual variations of the interplay of different energy scales over large distances, reflecting sensitively even the weakest interactions. Such spin textures have been of great fundamental and technological interest for many decades, ranging from field-theoretical questions to spintronics applications (6–8). For instance, great efforts have been dedicated to measurements of magnetic domains in bulk materials using polarized neutron imaging (9, 10), but the spatial resolution of a few micrometers achieved to date exceeds largely the atomic scales of interest. Much higher resolution has recently been reported using hard x-ray scattering in transmission geometry (11). However, for the micrometer-sized crystals required in these studies, surfaces dominate the scattering volume such that the link with genuine bulk properties cannot be addressed unambiguously. Moreover, a sophisticated reconstruction of the magnetization profile is required, making the interpretation of the experimental data rather demanding.

To clarify the effects of surfaces on the properties of a bulk material deep below a surface, skyrmions in chiral magnets are ideally suited from an experimental point of view, as the spins exhibit changes of orientation in all spatial directions. X-rays are perfectly matched to the length scales of the magnetic periodicities, suggesting that studies of the spin structure with increasing depth as controlled by the scattering angle or the photon energy, should be possible (12). In addition, representing chiral spin textures, the dichroism of soft x-ray scattering permits reconstruction of the full three-dimensional spin order, providing information on gradual variations (13, 14). Last but not least, high-quality single crystals are available as a key precondition for meaningful experimental results.

On a different note, skyrmion materials are also ideally suited for the investigation of the effects of surfaces on the bulk from a theoretical point of view, as a remarkably complete material-specific quantitative account has been developed (15–18). At the heart of the formation of skyrmions in bulk chiral magnets is a hierarchy of energy scales comprising, in decreasing strength, exchange interactions with coupling J, Dzyaloshinskii-Moriya (DM) spin-orbit interaction

Significance Statement

Magnetic skyrmion lattices have exceptional properties making them ideally suited for a new generation of spintronics devices. As devices are surface-dominated, a key question concerns the influence of surfaces on the spin structure. While a wide range of methods exist for studies of 2-dimensional skyrmions, the detailed knowledge of three-dimensional magnetic structures has remained elusive. Here we use tomographic resonant elastic x-ray scattering to reconstruct the depth dependence of a three-dimensional skyrmion crystal order in Cu_2OSeO_3. We find a continuous transformation with increasing depth from complete Néel-type winding at the surface to the Bloch-type winding in the bulk. Our study suggests the importance of free surfaces has been completely underestimated and will be of central importance for future skyrmionics applications.

S.L.Z., G.v.d.L., A.B., and T.H. performed the experiments and S.L.Z. developed the dichroism extinction rule for REXS. H.B. grew the sample, and J.M., M.G., and L.H. carried out the micromagnetic simulations. G.v.d.L. performed absorption calculations. S.L.Z., C.P., and T.H. wrote the manuscript with input from all authors. All authors discussed the results and reviewed the manuscript.

The authors declare no conflict of interest.

[1]To whom correspondence should be addressed. E-mail: thorsten.hesjedalphysics.ox.ac.uk

with coupling D, and higher-order crystal field terms. All of these interactions are controlled by the atomic positions and symmetries of the underlying crystal structure. While the ratio of the exchange coupling and the DM interaction, J/D generate changes of the spin orientation at a material-specific modulation length, $J/D \approx \lambda/2\pi$, the character of the DM interactions determines whether Bloch or Néel twisting is realized.

In our study we exploited that magnetic skyrmions are characterized by the topological winding number N and the helicity angle χ (see Fig. 1 for an illustration and the Methods section for the mathematical definition). As shown in Fig. 1 for the two abundant types of skyrmions observed experimentally in magnetic materials featuring $N = 1$, notably Bloch- and Néel-type skyrmions, the helicity angle χ assumes the values $\chi = \pm\pi/2$, and $\chi = 0$ or π, respectively. While the former stabilize in cubic chiral magnets such as MnSi (19), $Fe_{1-x}Co_xSi$ (20), FeGe (21), Cu_2OSeO_3 (22, 23), and $Co_xZn_yMn_z$ (24), the latter have been observed at surfaces and interfaces of thin film systems (25–28) as well as in bulk systems such as GaV_4S_8, and GaV_4Se_8, exhibiting strong uniaxial anisotropies and DM interactions akin to those in interfacial systems (29).

Taken together, an exceptionally complete understanding of different skyrmion hosting materials exists in terms of the underlying magnetic rigidities and associated static and dynamic properties. In particular, a universal account of the collective spin excitations across different magnetic phases for different materials has been reported (30–35), which reflects these rigidities. In turn, this allows detailed comparison, how perturbations of the magnetic state propagate in the bulk environment.

Surfaces represent such a perturbation of skyrmion hosting materials in two ways. First, atoms at the surface experience a different balance of local interactions, thus putatively permitting magnetic moments at the surface to assume energetically more favorable orientations as compared to the bulk (36, 37). Second, due to the lack of inversion symmetry of the surface additional interaction terms may be allowed by symmetry. While the former has been predicted theoretically but not been proven experimentally, the latter has been studied both theoretically and experimentally in thin films (25, 26) as well as heterostructures (18, 28).

As the interactions on all scales originate in the coupling of adjacent spins s_i and s_j, this propagation must be determined by the local atomic arrangement. Hence, according to the commonly accepted view that the surface affects the atomic positions in the top few atomic layers only, even the largest possible perturbation of the spin orientation, notably a tilt by 90° away from the original orientation, will essentially be determined by the interactions and associated magnetic rigidities of the bulk. In turn, for the case of helimagnetically modulated states with wavelength λ any perturbation may be expected to vanish at a distance $\sim J/D \approx \lambda/2\pi$, characteristic of the balance of the underlying interactions.

Recent theoretical and experimental studies have considered the importance of surfaces on the stability of skyrmions (38–42). The same energetics of surfaces has inspired the prediction of metastable states, so-called chiral bobbers (37), as putatively observed by holographic Lorentz transmission electron microscopy (LTEM) in selected cubic chiral magnets (42–44). However, for the thin lamella studied the interplay of the surface with the bulk cannot be unraveled. Moreover, an abundance of subtle structural and compositional defects introduced during the preparation of the samples cannot be ruled out.

To the best of our knowledge, the propagation of surface-induced changes of the spin orientation deep into the bulk at distances up to several hundred nm has not been studied experimentally before. In our study we have addressed this topic in terms of a quantitative comparison between the rigidities of the magnetic state, as inferred from the helimagnetic modulation length λ, with the propagation length of surface-induced Néel-twisting, as determined by the helicity angle χ, both recorded in the same measurement. As our main result we find that the Néel twisting propagates an order of magnitude deeper into the bulk than expected theoretically, i.e., the heuristically expected decay length $\lambda/2\pi$ and Néel decay length inferred from the helicity χ differ by an order of magnitude. This has far-reaching implications for the stabilization of skyrmions in surface dominated systems, as well as surface-induced materials properties even deep inside bulk materials.

Results

To overcome the limitations of conventional imaging and diffraction techniques in studies of the depth dependence of bulk materials at distances well below the surface, we performed resonant elastic x-ray scattering (REXS). By changing the energy of the incident x-rays, we varied systematically the attenuation depth to perform a quasi-tomographic mapping of the magnetic state. This goes well beyond previous depth-dependent REXS studies, which pursued chemical modifications and the identification of the presence of magnetic phases only (12, 14, 45).

For our study we chose single-crystal Cu_2OSeO_3, as high-quality single crystals are readily available and the material is known to be chemically and structurally stable and well-behaved. Typical experimental and calculated diffraction patterns are shown in Figs. 1 and 2, respectively. The hexagonally long-range ordered skyrmion lattice phase gives rise to a six-fold diffraction pattern, providing direct information on λ and thus the hierarchy of magnetic interactions (13, 46). Using the circular dichroism (CD) from all six magnetic skyrmion lattice peaks, i.e., the difference between the intensities obtained using left- and right-circularly polarized incident x-rays, an extinction direction of this diffraction pattern may be observed at which the dichroism vanishes (white arrows in Figs. 1 and 2). The orientation of the extinction direction corresponds directly to the helicity angle χ.

As the magnetic properties in Cu_2OSeO_3 originate in the magnetic moment of the Cu^{2+} ions, we tuned the photon energy across the Cu $L_{2,3}$ edge under the (001) diffraction condition (47). Details of the experimental geometry have been reported elsewhere (47) and may also be found in the Supplementary Materials. Further, the intensity patterns recorded experimentally for a given incident photon energy represent a weighted average over photons scattered at different depths. The attenuation profile of the intensity, taking into account the actual path length of the photons in the material under the given scattering angle, was determined by means of radiative transition probability calculations at the Cu $L_{2,3}$ edge and found to be essentially exponential (cf. Ref. (48) and Supplementary Materials). We carefully confirmed that parasitic signal contributions due the effects of natural dichroism and birefringence do not affect our results as discussed in the Supplementary Materials. For what follows, we define a sampling depth normal to the surface, d_a, representing the point where the scattering intensity has dropped to $1/e$, where d_a as a function of photon energy is shown in Fig. 2 A.

Data were recorded in the skyrmion phase under an applied magnetic field of 32 mT at a temperature of 57 K as a function of photon energy. All REXS diffraction patterns displayed the same basic orientation of the sixfold intensity pattern akin to the calculated patterns shown in Fig. 1 (C1) through (C4). In addition, all patterns displayed a well-defined extinction direction, which was found to change as a function of photon energy, characteristic of a helicity angle changing

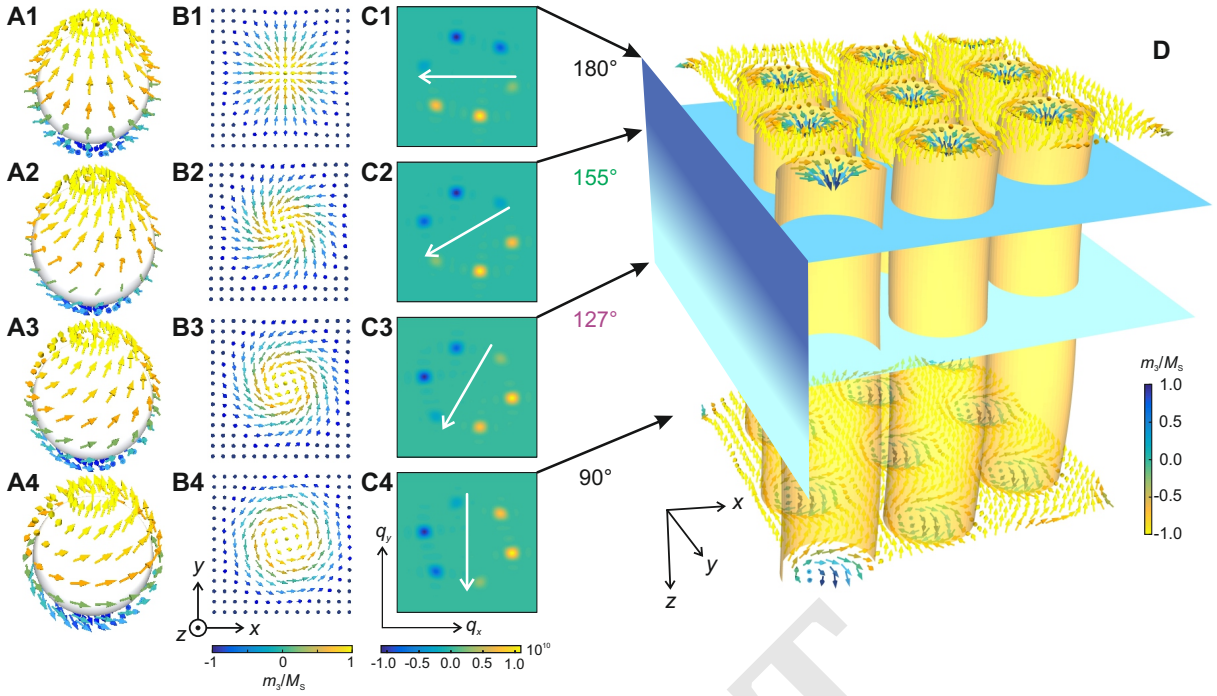

Fig. 1. Illustration of skyrmion order ranging from Néel to Bloch twisting with increasing depth below a surface. (*A1-A4*) Real-space hedgehog spin configuration on the surface of a sphere for skyrmions with winding number $N = 1$ varying between pure Néel-twisting (*A1*) and pure Bloch-twisting (*A4*). The surface of the spheres corresponds to order-parameter space. (*B1-B4*) Planar spin configuration varying between pure Néel-twisting (*B1*) and pure Bloch-twisting (*B4*). A stereographic projection connects the planar patterns shown in panels (*B1*) through (*B4*) with the hedgehog configurations shown in panels (*A1*) through (*A4*), respectively. (*C1-C4*) Calculated dichroic REXS diffraction pattern associated with a hexagonal lattice composed of the spin configurations shown in panels B1 through B4. The orientation of the extinction line marked by a white arrow corresponds to the helicity angle χ denoted on the right hand side of the panels. Consequently the chirality of the skyrmions can be straightforwardly determined (see Supplementary Materials). $\chi = 180°$ (*C1*) and $\chi = 90°$ (*C4*) correspond to pure Néel- and pure Bloch-twisting, respectively. (*D*) Schematic illustration of the change from Néel to Bloch twisting with increasing depth below the surface. The color coding reflects the z-direction of the magnetization.

with depth. Shown in Fig. 2 B is the helicity angle, χ_m as a function of energy determined directly from the measured diffraction patterns. The red curve in Fig. 2 B reflects the depth dependence as inferred self-consistently from the experimental data when taking into account the depth dependent intensity attenuation (see text and Fig. 3 for details).

Typical intensity patterns for 931.25 eV and 932.45 eV as associated with values of d_a of ∼31 nm and ∼77 nm featuring helicity angles of 155° and 127° are shown in Figs. 2 C and D, respectively. This suggests that the skyrmions are right-handed (see Supplementary Materials). All data were resolution-limited without indications of radial or azimuthal broadening, corresponding to $\lambda = 57.58\,\mathrm{nm}$ in excellent agreement with the literature (22). The lack of radial broadening as a function of photon energy implied that the magnetic modulation length λ, which is purely determined by the ratio of the exchange and DM interactions, did not change as a function of depth.

The change of χ_m as a function of energy reveals a variation of the skyrmion lattice between Néel and Bloch twisting with increasing depth. This may seem surprising, as an averaging of scattering intensities featuring gradual changes of χ with each layer contributing equally to the average would result in the loss of a well-defined extinction direction in the diffraction pattern. However, assuming a monotonic change of χ with increasing depth, where the intensity contributed by each layer is weighted according to an exponential attenuation profile as inferred from experiment, an intensity pattern with a well-defined extinction line is expected as illustrated in Figs. 2 E and F.

Shown in Fig. 3 A is the measured helicity angle χ_m as a function of sampling depth d_a (cf. Figs. 2 (A) and (B)). The orientation of the plot has been rotated to better emphasize the evolution with increasing depth, as qualitatively illustrated in Fig. 1 D. We note, that the experimental data oversample the underlying depth dependence $\chi_{exp}(z)$. The measured values $\chi_m(d_a)$ were fitted self-consistently, taking into account the energy dependent attenuation of the photon intensity. We assumed an exponential variation $\chi_{exp}(z) = (\chi^0_{exp} - 90°)\exp(-z/L_{exp}) + 90°$ with pure Bloch twisting ($\chi = 90°$) deep in the bulk. The helicity at the surface, χ^0_{exp}, and the helicity decay length, L_{exp} are fit parameters.

As shown in Fig. 3 B, we find $\chi^0_{exp} = 179.8°$ at the surface of the bulk sample, i.e., a pure Néel state. This Néel state changed monotonically into a pure Bloch state, $\chi(z) \to 90°$ on a helicity decay length $L_{exp} = 62.5\,\mathrm{nm}$. We note that the red line in Fig. 2 B and the diffraction patterns in Figs. 2 E and F, take into account $\chi_{exp}(z)$ as shown in Fig. 3 B.

Discussion

The helicity decay length observed experimentally, $L_{exp} = 62.5\,\mathrm{nm}$, seems deceptively close to the magnetic modulation length $\lambda = 57.58\,\mathrm{nm}$. However, as emphasized above the relaxation is heuristically expected to occur on a length scale $\lambda/2\pi \approx 9.1\,\mathrm{nm}$, i.e., it is expected to occur on a distance that is significantly shorter than experimentally observed. Moreover, numerical calculations of the effects of surfaces have recently established that the presence of a magnetic field additionally modifies the decay length to be expected (40).

To obtain deeper insights, we have therefore carried out material-specific numerical calculations of the helicity decay length, L_{th}, tak-

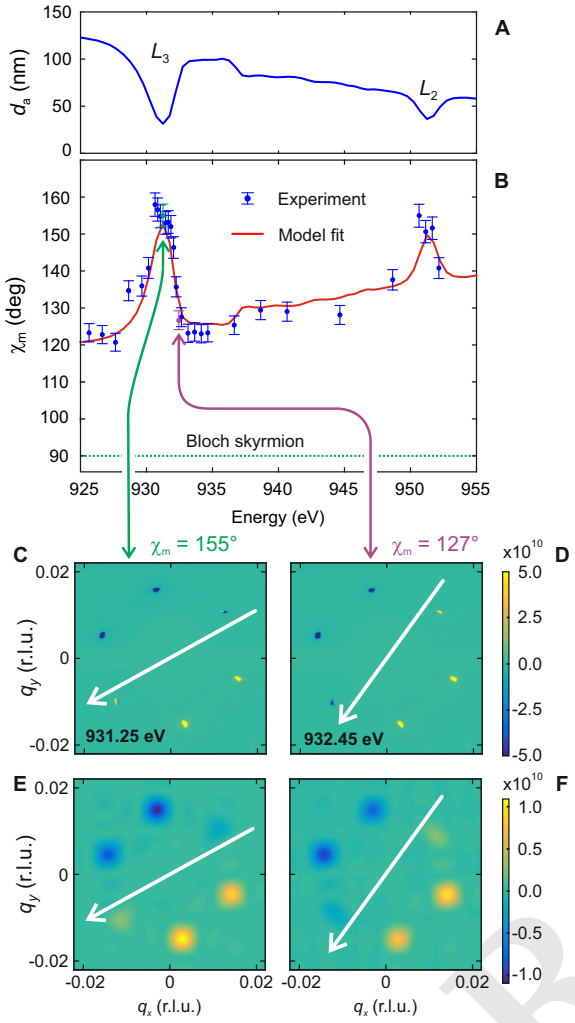

Fig. 2. Key aspects of polarized REXS for the determination of the depth dependence of skyrmion lattice order in Cu_2OSeO_3. (*A*) Energy dependence of the penetration depth of photons tuned to the Cu $L_{2,3}$ edge under the (001) diffraction condition in Cu_2OSeO_3, where d_a corresponds to the depth at which the scattering intensity has decreased to $1/e$. (*B*) Helicity angle χ_m as a function of photon energy taken directly from the measured REXS diffraction pattern. The red line corresponds to the depth dependence as inferred self-consistently from the experimental data (see text for details and Fig. 3). (*C,D*) Typical experimental REXS intensity pattern observed for photon energies of 931.25 eV and 932.45 eV, respectively. All patterns recorded experimentally were resolution limited with a well-defined extinction direction (white arrow). (*E,F*) Calculated REXS intensity pattern based on the intensity attenuation profile taking into account the depth dependence inferred from the experiment (cf. Fig. 3).

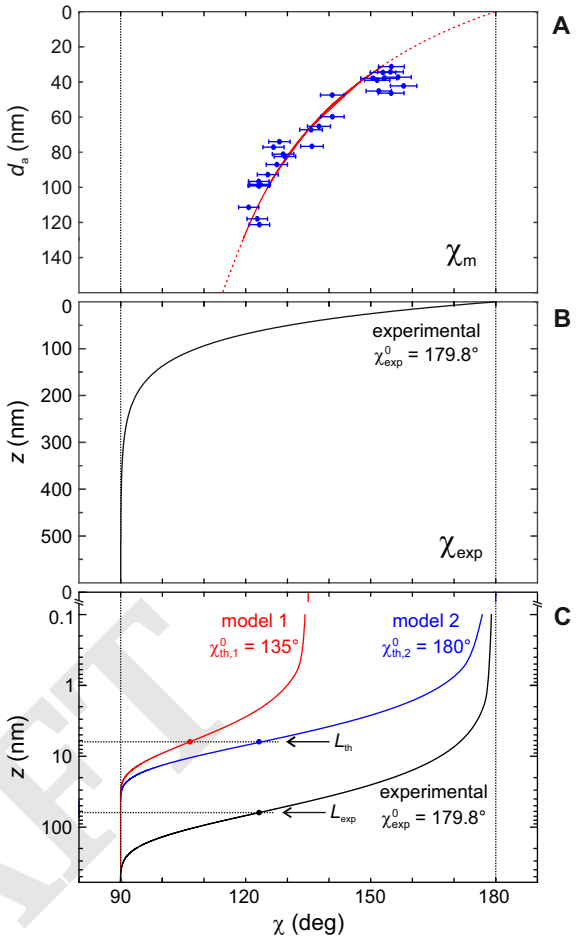

Fig. 3. Depth dependence of skyrmion helicity in Cu_2OSeO_3. Pure Néel-twisting at the surface penetrates deep into the bulk and turns into pure Bloch-twisting below several hundred nanometers. (*A*) Attenuation depth d_a versus measured helicity angle χ_m as shown in Figs. 2*A* and 2*B*, respectively. The red line represents the depth dependence of $\chi_{\rm exp}$, taking into account self-consistently the energy dependence of the intensity attenuation with increasing depth. (*B*) Depth dependence of the helicity angle in Cu_2OSeO_3 determined experimentally (this corresponds to the red curve in panel (*A*)). Pure Néel-twisting ($\chi^0_{\rm exp} = 179.8°$) at the surface ($z = 0$) changes exponentially into pure Bloch-twisting ($\chi_{\rm exp} = 90°$) below several hundred nanometers. (*C*) Comparison of $\chi_{\rm exp}$ with material-specific calculations. The experimentally observed helicity decay length is $L_{\rm exp} = 62.5\,{\rm nm}$. Model 1 considers an unconstrained surface. For the interaction strength J/D taken from the experimentally determined value of λ two major differences are observed: (i) Néel-twisting at the surface is much weaker ($\chi^0_{\rm th,1} = 135° \ll \chi^0_{\rm exp} = 179.8°$), and (ii) Bloch twisting is reached much faster, where $L_{\rm th} = 5.4\,{\rm nm}$. Model 2 assumes pure Néel twisting at the surface ($\chi^0_{\rm th,2} = 180°$), where $L_{\rm th} = 5.4\,{\rm nm}$ is the same as for model 1.

ing into account the exchange interactions, $J\vec{S}_i \cdot \vec{S}_j$, the isotropic DM interaction in a cubic crystal structure, $\vec{D}_{ij} \cdot (\vec{S}_i \times \vec{S}_j)$, and the effects of dipolar interactions (49, 50). The absence of radial broadening of the diffraction spots implies that the ratio J/D did not change as a function of depth. Since it seemed extremely unlikely that both interactions change such that the ratio is unaltered, this suggested also that the interactions are quantitatively unchanged with increasing depth.

In our calculations we focused on two scenarios. Model 1 considered an unconstrained surface, whereas model 2 assumed a pure Néel state at the surface. The latter may be justified with the presence of additional DM terms due to the symmetries of the surface, referred to as interfacial DMI. Details of the numerical implementation may be found in the supplementary online information. Shown in Fig. 3 C is a comparison of $\chi_{\rm exp}(z)$ with key results of our calculations. In both models we found that the Néel twisting at the surface changed into Bloch twisting in the bulk following essentially an exponential depth dependence in excellent qualitative agreement with experiment.

However, in model 1 the helicity angle at the surface stabilized at $\chi^0_{\rm th,1} \approx 135°$ and the Néel-twisting extended into the bulk with a helicity decay length $L_{\rm th} \approx 5.4\,{\rm nm}$. Thus, $\chi^0_{\rm th}$ as well as $L_{\rm th}$ for the unconstrained surface (model 1) were much smaller than experiment. Further, when forcing the surface to exhibit pure Néel twisting (model 2), we also found the same short helicity decay length $L_{\rm th} \approx 5.4\,{\rm nm}$. Observation of the same value of $L_{\rm th}$ in model 1

and 2 is not surprising, as the bulk properties are expected to control the decay length of a perturbation of the magnetic state as explained above.

It is important to note that the theoretical and experimental curves in Fig. 3 C are roughly parallel, i.e., the difference is over an order of magnitude, regardless of the precise helicity angle reached. Thus, the results of our calculations underscore the heuristic argument that the propagation of perturbations into the bulk is determined by the balance of exchange and DM interactions and vanish at distances of order $\lambda/2\pi$. In fact, the difference between theory and experiment is over an order of magnitude taking into account the effect of the applied field (40). The long-range character of dipolar interactions, having been included in our calculations, does not change these conclusions. This raises the questions, first, whether these effects are specific to the skyrmion lattice order, and, second, in which way the rigidity of the magnetic order in the bulk may be affected by the surface?

Unfortunately, for the scattering and magnetic field geometries accessible with our experimental set-up, it was not possible to obtain comparable information on the depth dependence of any of the other magnetic phases. However, it is interesting to note, that Lorentz TEM holography has recently been reported for FeGe and $Fe_{0.95}Co_{0.05}Ge$ (41, 51). In these studies Néel-twisting is observed on the surfaces (top and bottom) of a thin lamella. Unnoticed by the authors of these studies, the data reported in these papers entail the same discrepancies we report here for bulk Cu_2OSeO_3 using REXS. However, as pointed out above the sample geometry required for LTEM is different and changes of the crystal structure as well as defects due to the thinning process cannot be ruled out.

Further, the resolution-limited evidence that the modulation length as a function of photon energy and associated probing depth does not change, renders local changes of the microscopic interactions due to changes of the atomic positions highly unlikely. This includes surface-induced magnetic anisotropy, which may not cause a change from Néel to Bloch twisting. These considerations point at a dynamic origin of the softening of the magnetic rigidity as most likely explanation, e.g., due thermal fluctuations or magneto-elastic coupling.

Concerning the effects of thermal fluctuations we note that a remarkably complete theoretical and experimental understanding of spin waves in cubic chiral magnets has been developed, including Cu_2OSeO_3 (30, 31, 34, 35, 52–54). This includes the effects of critical fluctuations within a Brazovskii scenario of a fluctuation-induced first order transition and the stabilization of the skyrmion phase by virtue of thermal Gaussian fluctuations (55, 56). However, when we explored the effects of finite temperatures in our calculations, we did not find any indications of substantial changes of the helicity angle at the surface as well as the helicity decay length. A different mechanism may be connected to the effects of magneto-elastic coupling. Here Raman studies in the related compound MnSi (57) suggest unusual magnon-phonon coupling effects. Unfortunately, quantitative experimental and theoretical exploration of this possibility is well beyond the scope of our study and motivates further investigation planned for the future.

In summary, determining the full three-dimensional spin order in the skyrmion lattice of Cu_2OSeO_3 by means of polarized REXS as a depth dependent probe, we find pure Néel twisting at the surface that changes gradually into pure Bloch twisting deep within the bulk. Combining our results with material specific modeling, we are forced to conclude that surfaces affect the properties even at distances up to several hundred atomic layers. These effects are of great importance when tailoring skyrmions in nano-scaled systems, as surfaces appear to favor skyrmions energetically much stronger than anticipated theoretically (38–41).

Whereas early work considered the formation of hexagonal skyrmion lattices purely as the result of a minimization of the total energy (19, 58, 59), recent studies address the additional effects of symmetry breaking of surfaces or strain-imposed modifications of the interactions. For instance, an edge twist effect was proposed and putatively observed, causing a canting of the magnetization along the boundary of a specimen that potentially stabilizes individual skyrmions, skyrmion clusters, and skyrmion chains (39, 60–62). Further, it has been argued that surface confinement in combination with finite system thickness affects the equilibrium regime of the skyrmion lattice phase uniformly, causing twisted helicity angles and extra modulations along the thickness (36, 41, 63). Even non-axisymmetric 3D skyrmion modulations (64–67), as well as metastable surface configurations referred to as chiral bobbers, have been proposed (37, 63, 68). It is important to emphasize that none of these mechanisms explains our findings. On the contrary, our observations of a much stronger Néel twisting induced by the surface of a bulk crystal than anticipated theoretically, imply that all of these effects may be much stronger quantitatively than anticipated.

In view that microscopic methods such as as LTEM, magnetic force microscopy, and scanning tunneling microscopy used so far in studies of nanoscale systems hosting skyrmions provide information on selected magnetization components only, quantitative tomography of the full 3D structure will be essential. Here, REXS offers a new avenue, providing direct access to depth-resolved information of the chirality and helicity even for small scattering volumes. This represents an important methodological step forward as it permits to study, e.g., a possible attractive nature of skyrmion tubes in thin platelets where soft x-rays are able to probe the entire thickness of the specimen, permitting the full reconstruction of the skyrmion characteristics.

On a final note, our results may also have far-reaching implications for the general understanding of structure versus functionality relationships beyond the magnetic textures investigated here. Namely, they indicate that surfaces play a much more important role than hitherto assumed. This motivates the experimental and theoretical investigation of the precise atomic structure and associated dynamical properties in bulk materials deep below their surface, representing unchartered territory.

Materials and Methods

Sample. Single crystalline Cu_2OSeO_3 was grown by chemical vapor transport, and subsequently characterized by single crystal diffraction (using Cu $K\alpha$ radiation) and electron backscattering diffraction, in order to confirm the crystal quality and single-chirality. A carefully polished (001)-surface was used for the REXS experiments, which were carried out at the RASOR diffractometer on beamline I10 at the Diamond Light Source (UK).

Skyrmion lattice phase. In the skyrmion lattice phase (i.e., at 57 K and in an applied field of 32 mT along the [001]-direction), the six magnetic peaks appear as satellites surrounding the (0,0,1) Bragg peak, with the modulation wavevector $q = 0.0158$ r.l.u. In the $(hk1)$-plane, the azimuthal angles Ψ_i describe the orientation of the wavevectors $\mathbf{q}_i$, where $i = 1, 2, \ldots, 6$ and $\Psi_{i+1} = \Psi_i + 60^\circ$, with $\Psi \in [-180^\circ, 180^\circ)$. The coordinate system is illustrated in Fig. 2, in which we define $\Psi = 0^\circ$ along the q_x direction (see also Supplementary Figure S2).

CD-REXS technique. For the purpose of our study, we define the circular dichroism signal (the CD-REXS signal) as the difference in diffraction intensities for the same skyrmion peak at the same geometrical condition, as obtained using left- and right-circularly

polarized soft x-rays. In our experiment, the CD-REXS was recorded by integrating a series of reciprocal-space-map scans for each polarization separately, followed by normalization and subsequent subtraction of the left- and right-circularly polarized patterns (for details see refs. (13, 47, 69)). The direct CD-REXS pattern shows six magnetic peaks with varying CD amplitudes $I_{\mathrm{CD}}(\Psi)$, and a distinct boundary that separates the positive and negative halves. In the $(hk1)$-plane, the extinction vector that characterizes the boundary always passes through the center of the plane [i.e., the (0,0,1) reciprocal space point], and its direction varies with photon energy. Its physical meaning is further discussed in the Supplementary Materials.

ACKNOWLEDGMENTS. We wish to thank A. Rosch for stimulating discussions and S. Maier and the staff at the Diamond Light Source for support. The resonant soft x-ray scattering experiments were carried out on beamline I10 at the Diamond Light Source, UK, under proposal SI-11784. S.L.Z. and T.H. acknowledge financial support by the Semiconductor Research Corporation (SRC) and EPSRC (EP/N032128/1). J.M. and L.H. acknowledge financial support by DFG CRC 1238 (project C04). J.M. also thanks the Deutsche Telekom Stiftung and the Bonn-Cologne Graduate School of Physics and Astronomy for financial support. M.G. was supported by DFG CRC 1143 and DFG grant GA 1072/5-1. A.B. and C.P. acknowledge financial support through DFG TRR80 (projects E1 and F7) and ERC Advanced Grant 291079 (TOPFIT).

1. Hellman F, et al. (2017) Interface-induced phenomena in magnetism. *Rev. Mod. Phys.* 89(2):025006.
2. Hudson JB (1998) *Surface Science: An Introduction.* (Wiley-Interscience).
3. Blavette D, Vurpillot F, Deconihout B, Menand A (2011) *Atom Probe Tomography: 3D Imaging at the Atomic Level* eds. Lasagni F, Lasagni A. (Springer, Berlin, Heidelberg).
4. Kelly TF (2017) Atomic-scale analytical tomography. *Microscopy and Microanalysis* 23(1):34–45.
5. Baruchel J, et al. (2006) Advances in synchrotron radiation microtomography. *Scripta Materialia* 55:41–46.
6. Hubert A, Schäfer R (2008) *Magnetic Domains - The Analysis of Magnetic Microstructures.* (Springer).
7. Sander D, et al. (2017) The 2017 magnetism roadmap. *J. Phys. D: Appl. Phys.* 50:363001.
8. Žutić I, Fabian J, Das Sarma S (2004) Spintronics: Fundamentals and applications. *Rev. Mod. Phys.* 76:323–410.
9. Manke I, et al. (2010) Three-dimensional imaging of magnetic domains. *Nat. Commun.* 1:125.
10. Schulz M, et al. (2010) Towards a tomographic reconstruction of neutron depolarization data. *J. Phys. Conf. Ser.* 211:012025.
11. Donnelly C, et al. (2017) Three-dimensional magnetization structures revealed with x-ray vector nanotomography. *Nature* 547:328.
12. Dürr HA, et al. (1999) Chiral magnetic domain structures in ultrathin FePd films. *Science* 284:2166.
13. Zhang SL, van der Laan G, Hesjedal T (2017) Direct experimental determination of spiral spin structures via the dichroism extinction effect in resonant elastic soft x-ray scattering. *Phys. Rev. B* 96:094401.
14. Chauleau JY, et al. (2018) Chirality in magnetic multilayers probed by the symmetry and the amplitude of dichroism in x-ray resonant magnetic scattering. *Phys. Rev. Lett.* 120(3):037202.
15. Nagaosa N, Tokura Y (2013) Topological properties and dynamics of magnetic skyrmions. *Nat. Nanotechnol.* 8:899.
16. Bauer A, Pfleiderer C (2016) *Generic Aspects of Skyrmion Lattices in Chiral Magnets.* (Springer International Publishing, Cham), pp. 1–28.
17. Wiesendanger R (2016) Nanoscale magnetic skyrmions in metallic films and multilayers: A new twist for spintronics. *Nat. Rev. Mater.* 1:16044.
18. Sampaio J, Cros V, Rohart S, Thiaville A, Fert A (2013) Nucleation, stability and current-induced motion of isolated magnetic skyrmions in nanostructures. *Nat. Nanotechnol.* 8:839.
19. Mühlbauer S, et al. (2009) Skyrmion lattice in a chiral magnet. *Science* 323:915.
20. Yu XZ, et al. (2010) Real-space observation of a two-dimensional skyrmion crystal. *Nature* 465:901.
21. Yu XZ, et al. (2011) Near room-temperature formation of a skyrmion crystal in thin-films of the helimagnet FeGe. *Nat. Mater.* 10:106.
22. Adams T, et al. (2012) Long-wavelength helimagnetic order and skyrmion lattice phase in Cu_2OSeO_3. *Phys. Rev. Lett.* 108:237204.
23. Seki S, Yu XZ, Ishiwata S, Tokura Y (2012) Observation of skyrmions in a multiferroic material. *Science* 336:198.
24. Tokunaga Y, et al. (2015) A new class of chiral materials hosting magnetic skyrmions beyond room temperature. *Nat. Commun.* 6:7638.
25. Heinze S, et al. (2011) Spontaneous atomic-scale magnetic skyrmion lattice in two dimensions. *Nat. Phys.* 7:713–718.
26. Romming N, et al. (2013) Writing and deleting single magnetic skyrmions. *Science* 341:636.
27. Jiang W, et al. (2015) Blowing magnetic skyrmion bubbles. *Science* 349(6245):283–286.
28. Moreau-Luchaire C, et al. (2016) Additive interfacial chiral interaction in multilayers for stabilization of small individual skyrmions at room temperature. *Nat. Nanotechnol.* 11(5):444–448.
29. Kézsmárki I, et al. (2015) Néel-type skyrmion lattice with confined orientation in the polar magnetic semiconductor GaV_4S_8. *Nat. Mater.* 14(11):1116–1122.
30. Okamura Y, et al. (2013) Microwave magnetoelectric effect via skyrmion resonance modes in a helimagnetic multiferroic. *Nat. Commun.* 4:2391.
31. Seki S, et al. (2016) Magnetochiral nonreciprocity of volume spin wave propagation in chiral-lattice ferromagnets. *Phys. Rev. B* 93(23):235131.
32. Janoschek M, Jonietz F, Link P, Pfleiderer C, Böni P (2010) Helimagnons in the skyrmion lattice of MnSi. *J. Phys.: Conf. Ser.* 200(3):032026.
33. Schwarze T, et al. (2015) Universal helimagnon and skyrmion excitations in metallic, semiconducting and insulating chiral magnets. *Nat. Mater.* 14:478.
34. Stasinopoulos I, et al. (2017) Linearly polarized GHz magnetization dynamics of spin helix modes in the ferrimagnetic insulator Cu_2OSeO_3. *Sci. Rep.* 7:7037.
35. Stasinopoulos I, et al. (2017) Low spin wave damping in the insulating chiral magnet Cu_2OSeO_3. *Appl. Phys. Lett.* 111:032408.
36. Rybakov FN, Borisov AB, Bogdanov AN (2013) Three-dimensional skyrmion states in thin films of cubic helimagnets. *Phys. Rev. B* 87:094424.
37. Rybakov FN, Borisov AB, Blügel S, Kiselev NS (2015) New type of stable particlelike states in chiral magnets. *Phys. Rev. Lett.* 115:117201.
38. Rohart S, Thiaville A (2013) Skyrmion confinement in ultrathin film nanostructures in the presence of Dzyaloshinskii-Moriya interaction. *Phys. Rev. B* 88:184422.
39. Meynell SA, Wilson MN, Fritzsche H, Bogdanov AN, Monchesky TL (2014) Surface twist instabilities and skyrmion states in chiral ferromagnets. *Phys. Rev. B* 90:014406.
40. Müller J, Rosch A, Garst M (2016) Edge instabilities and skyrmion creation in magnetic layers. *New J. Phys.* 18:065006.
41. Leonov AO, et al. (2016) Chiral surface twists and skyrmion stability in nanolayers of cubic helimagnets. *Phys. Rev. Lett.* 117:087202.
42. Zheng F, et al. (2017) Experimental observation of magnetic bobbers for a new concept of magnetic solid-state memory. *arxiv:* p. 1706.04654v1.
43. Jin C, et al. (2017) Control of morphology and formation of highly geometrically confined magnetic skyrmions. *Nat. Commun.* 8:15569.
44. Wild J, et al. (2017) Entropy-limited topological protection of skyrmions. *Sci. Adv.* 3:e1701704.
45. Fink J, Schierle E, Weschke E, Geck J (2013) Resonant elastic soft x-ray scattering. *Rep. Prog. Phys.* 76:056502.
46. Zhang SL, et al. (2016) Multidomain skyrmion lattice state in Cu_2OSeO_3. *Nano Lett.* 16:3285–3291.
47. Zhang SL, et al. (2016) Resonant elastic x-ray scattering from the skyrmion lattice in Cu_2OSeO_3. *Phys. Rev. B* 93(21):214420.
48. Cowan RD (1981) *The theory of atomic structure and spectra.* (University of California Press, Berkeley).
49. Buhrandt S, Fritz L (2013) Skyrmion lattice phase in three-dimensional chiral magnets from Monte Carlo simulations. *Phys. Rev. B* 88:195137.
50. Milde P, et al. (2013) Unwinding of a skyrmion lattice by magnetic monopoles. *Science* 340:1076–1080.
51. Schneider S, et al. (2017) Induction mapping of the 3d spin texture of Bloch-Néel skyrmions in thin helimagnets. *arXiv* p. 1710.08322.
52. Mochizuki M (2012) Spin-wave modes and their intense excitation effects in skyrmion crystals. *Phys. Rev. Lett.* 108:017601.
53. Schmakat P, et al. (2015) Spin dynamics and spin freezing at ferromagnetic quantum phase transitions. *Eur. Phys. J. Special Topics* 224:1041–1060.
54. Kindervater J, et al. (2014) Critical spin-flip scattering at the helimagnetic transition of MnSi. *Phys. Rev. B* 89:180408.
55. Brazovskii SA (1975) Phase transition of an isotropic system to a nonuniform state. *Sov. Phys. JETP* 41:85.
56. Janoschek M, et al. (2013) Fluctuation-induced first-order phase transition in Dzyaloshinskii-Moriya helimagnets. *Phys. Rev. B* 87:134407.
57. Eiter HM, et al. (2014) Raman study of the temperature and magnetic-field dependence of the electronic and lattice properties of MnSi. *Phys. Rev. B* 90:024411.
58. Rößler UK, Leonov AA, Bogdanov AN (2011) Chiral skyrmionic matter in non-centrosymmetric magnets. *J. Phys.: Conf. Ser.* 303:012105.
59. Park HS, et al. (2014) Observation of the magnetic flux and three-dimensional structure of skyrmion lattices by electron holography. *Nat. Nanotechnol.* 9:337.
60. Zheng F, et al. (2017) Direct imaging of a zero-field target skyrmion and its polarity switch in a chiral magnetic nanodisk. *Phys. Rev. Lett.* 119:197205.
61. Zhao X, et al. (2016) Direct imaging of magnetic field-driven transitions of skyrmion cluster states in fege nanodisks. *Proc. Natl. Acad. Sci. U.S.A.* 113:4918–4923.
62. Du H, et al. (2015) Edge-mediated skyrmion chain and its collective dynamics in a confined geometry. *Nat. Commun.* 6:8504.
63. Rybakov FN, Borisov AB, Blügel S, Kiselev NS (2016) New spiral state and skyrmion lattice in 3D model of chiral magnets. *New J. Phys.* 18:045002.
64. Leonov AO, Loudon JC, Bogdanov AN (2016) Spintronics via non-axisymmetric chiral skyrmions. *Appl. Phys. Lett.* 109:172404.
65. Leonov AO, Monchesky TL, Loudon JC, Bogdanov AN (2016) Three-dimensional chiral skyrmions with attractive interparticle interactions. *J. Phys. Condens. Matter* 28:35LT01.
66. Loudon JC, Leonov AO, Bogdanov AN, Hatnean MC, Balakrishnan G (2018) Direct observation of attractive skyrmions and skyrmion clusters in the cubic helimagnet Cu_2OSeO_3. *Phys. Rev. B* 97(13):134403.
67. Du H, et al. (2018) Interaction of individual skyrmions in a nanostructured cubic chiral magnet. *Phys. Rev. Lett.* p. arXiv:1804.02413.
68. Zheng F, et al. (2018) Experimental observation of chiral magnetic bobbers in B20-type FeGe. *Nat. Nanotechnol.*
69. Zhang SL, van der Laan G, Hesjedal T (2017) Direct experimental determination of the topological winding number of skyrmions in Cu_2OSeO_3. *Nat. Commun.* 8:14619.